crystals

MDPI

*Article*

# Effect of Nonmagnetic Hf Addition on Magnetic Properties of Melt-Spun Misch Metal-Fe-B Ribbons

**Mihaela Lostun, Marian Grigoraș *, Luiza C. Budeanu, Tiberiu Roman, Gabriela Buema, Gabriel Ababei, George Stoian and Nicoleta Lupu**

National Institute of Research and Development for Technical Physics, 47 Prof. Dimitrie Mangeron Blvd., 700050 Iasi, Romania; mlostun@phys-iasi.ro (M.L.); lbudeanu@phys-iasi.ro (L.C.B.); troman@phys-iasi.ro (T.R.); gbuema@phys-iasi.ro (G.B.); gababei@phys-iasi.ro (G.A.); gstoian@phys-iasi.ro (G.S.); nicole@phys-iasi.ro (N.L.)
* Correspondence: mgrigoras@phys-iasi.ro

**Abstract:** Misch Metal (MM)-Fe-B magnets are proposed to develop permanent magnets with a high performance/cost ratio and to balance the disproportionate use of rare earth (RE) resources. To improve the magnetic performance of (MM)-Fe-B ribbons precursors of magnets, the addition of non-magnetic hafnium (Hf) was used. $MM_{14}Fe_{80-x}Hf_xB_6$ (x = 0–3 at. %) ribbons were fabricated by melt-spinning technique at a wheel velocity of 35 m/s and were then annealed to obtain a nanocrystalline structure. The ribbons' magnetic properties, morphology, and structure were investigated methodically. It was found that the coercivity, Hc, of the $MM_{14}Fe_{80-x}Hf_xB_6$ (x = 0–3 at. %) as-spun ribbons increased significantly from 5.85 kOe to 9.25 kOe with an increase in the Hf content from 0 to 2 at. %, while the remanence decreased slightly for the whole 0–3 range at. % Hf. The grain size of the $RE_2Fe_{14}B$ phase gradually decreased as the Hf addition content increased from 0 to 3 at. %. As a result, the best combination of magnetic properties, such as Hc = 9.25 kOe, Mr = 87 emu/g, and maximum energy product $(BH)_{max}$ = 9.75 MGOe, was obtained in the ribbons with 2 at. % Hf addition was annealed at an optimal temperature of 650 degrees Celsius for 20 min. This work can serve as a useful reference for the further development of a new permanent magnet based on MM and Hf elements and can provide a feasible way for the efficient use of rare earth resources.

**Keywords:** RE-Fe-B magnets; Hf addition; magnetic properties; X-ray diffraction; thermal stability; differential scanning calorimetry

check for updates

**Citation:** Lostun, M.; Grigoraș, M.; Budeanu, L.C.; Roman, T.; Buema, G.; Ababei, G.; Stoian, G.; Lupu, N. Effect of Nonmagnetic Hf Addition on Magnetic Properties of Melt-Spun Misch Metal-Fe-B Ribbons. *Crystals* **2024**, *14*, 517. https://doi.org/10.3390/cryst14060517

Academic Editor: Jan Macutkevic

Received: 26 April 2024
Revised: 21 May 2024
Accepted: 27 May 2024
Published: 29 May 2024

**Copyright:** © 2024 by the authors. Licensee MDPI, Basel, Switzerland. This article is an open access article distributed under the terms and conditions of the Creative Commons Attribution (CC BY) license (https://creativecommons.org/licenses/by/4.0/).

## 1. Introduction

In the last two decades, permanent magnets (PMs) have become vital components used in advanced electronics systems, military applications, and emerging green energy technologies like hybrid electric vehicles (HEV), e-bikes, vans, and even heavy-duty vehicles and wind turbines [1–3]. The required physical characteristics for a high-performance permanent magnet are a high energy product $(BH)_{max}$ and a high Curie temperature (the temperature at which the ferromagnetic order disappears). The most powerful permanent magnets with a maximum energy product of $(BH)_{max}$ = 59 MGOe and the most used magnets available today are based on NdFeB-type alloys [4,5]. However, at high temperatures (T > 200 °C), these magnets show poor magnetic properties, and permanent magnet manufacturers usually add other rare earth metals with the potential to improve magnetic properties [6], including dysprosium (Dy), praseodymium (Pr), and terbium (Tb), especially to increase the operating temperature. As the exponential growth in demand for rare earths has far outstripped supply, these elements have become economic risk materials. At this time, the permanent magnet market is dominated 90% by NdFeB and hard ferrites magnets, in a ratio of 2:1. The interval between the upper limit of energy product of the ferrites (5.5 MGOe) and the lower limit of the energy product of the NdFeB magnets (35 MGOe) is currently vacant. However, several applications that need magnets

with $(BH)_{max}$ in this range (e.g., the robotics industry) are forced to use NdFeB magnets. Therefore, from an economic point of view, the development of a new type of magnet to fill this gap is also required, given that the robotics industry, for example, will explode in the coming years. Replacement of critical rare earth elements such as Nd, Dy, and Pr in RE-Fe-B with another non-critical rare earth that does not require separation; misch-metal (MM), which is an ore with a natural ratio of 25–35 wt. % La, 45–55 wt. % Ce, 4–10 wt. % Pr, and 14–18 wt. % Nd, has become a hot topic in the study of rare earth permanent magnets in recent years [7–12]. Hence, the elimination of the separation and purification of rare earth processes, which cause environmental pollution, results in a significant reduction in the cost and waste [13–16]. However, the total replacement of Nd with MM leads to the degradation of the magnetic properties [17], e.g., the Curie temperature (Tc) decreases by 30%, and there is also a significant decrease in saturation magnetization (Ms) and hence energy product [17,18]. Current approaches are limited to replacing Nd with MM without providing further solutions to improve Curie temperature and increase saturation magnetization [19]. In the case of Nd-Fe-B or Sm-Co permanent magnets, it has been observed that the magnetic properties can be improved by adding metal transition elements such as Ta, Ti, Zr, Hf, Mo, and Nb [20–29]. In the case of Hf, for example, the magnetic properties of the Nd-Fe-B alloy were reported to be improved as a result of the induction of magnetic anisotropy [21,30]. Chang reported that in SmCo7 alloys, the use of Hf substitution leads to an increase in coercivity and the energy product as a result of the increase in the anisotropy field of the 1:17 phase [31]. It has also been reported that the addition of Hf can effectively inhibit the formation of $\alpha$-Fe and the growth of $RE_2Fe_{14}B$ phase volume in low Nd content NdFeB nanocomposite permanent magnetic alloys [20]. The addition of Hf in the alloys with Nd content near the stoichiometry composition of $Nd_2Fe_{14}B$ can effectively refine the grain size and promote a more uniform nanostructure, thereby improving the magnetic properties and thermal stability [32]. Although the beneficial effects of Hf addition on the magnetic properties of Nd-Fe-B and their derivatives alloys have been studied, there has been no report on the Hf addition in MM-Fe-B alloys until now. Therefore, we expect that the addition of Hf to the MM-Fe-B compound will also have a beneficial effect on the magnetic properties.

In this paper, we investigate the effect of Hf addition on the structure and magnetic properties of the $MM_{14}Fe_{80-x}Hf_xB_6$ (x = 0–3 at. %) ribbons prepared by the melt-spinning method and establish a process route to improve the magnetic properties.

## 2. Materials and Methods

The process of melt-spinning was employed to produce ribbons through a two-step procedure. Initially, an ingot with a nominal composition of $MM_{14}Fe_{80-x}Hf_xB_6$ (x = 0–3 at. %) was prepared using the vacuum arc-melting method. The raw materials used for this process included MM with a purity of 99.5%, as well as Fe, Hf, and B with a purity greater than 99.99%. The misch-metal used in this process is composed of La-25%, Ce-53%, Pr-5%, and Nd-17%. The ingots were remelted four times under high vacuum conditions by turning them upside down and stirring to ensure uniform melting and homogeneous composition. In the second stage, the ingot underwent the melt-spinning process utilizing a melt-spinner equipped with a copper wheel measuring approximately 20 centimetres in diameter. The approximate weight of the alloy ingot was $5 \pm 0.2$ g, which was then crushed into small pieces and loaded into a quartz crucible with a V-shaped end and a nozzle diameter of $0.7 \pm 0.1$ mm. The ingot was melted using high-frequency induction up to $1250 \pm 5$ Celsius degrees under a high-purity argon atmosphere (about 0.6 bar), with the temperature inside the crucible being continuously monitored by a MAURER digital infrared pyrometer (Dr. Georg Maurer GmbH, Kohlberg, Germany). The distance between the quartz crucible and the copper cooling wheel surface was maintained at approximately $2 \pm 0.02$ mm, with the wheel speed being 35 m/s (linear speed) for all ribbons. The molten alloy was exposed to an argon pressure of 3 bar and ejected from the quartz tube onto the copper wheel, quickly solidifying in the form of ribbons upon contact with it. The ribbons

manufactured exhibited an amorphous structure and dimensions of 20 to 25 micrometres in thickness and 700 ± 5 µm in width. The selection of the initial composition, $MM_{14}Fe_{80}B_6$, and the starting speed were determined based on our previous experiments for the production of ribbons with an amorphous structure using RE-Fe-B [33,34]. In order to produce a well-ordered nanocrystalline structure, as-spun ribbons with an amorphous structure, which were generated through melt-spinning, were subjected to vacuum annealing at a pressure of approximately $5 \times 10^{-6}$ mbar. The temperature for this process was adjusted between 550 and 690 Celsius degrees, and the duration of the treatment was maintained for periods of 10 to 30 min. This precise process allowed for the identification of the optimal treatment temperature. The structure and morphology of the melt-spun ribbons were analyzed using X-ray diffraction (XRD) on a Bruker AXS D8-Advance diffractometer (Bruker, Mannheim, Germany), with Cu-Kα radiation, and scanning electron microscopy (SEM), FIB/FE-SEM Cross-Beam NEON 40 EsB, (Carl Zeiss Microscope GmbH, Oberkochen, Germany). Crystalline grain size was determined by the Debye–Scherrer method using DIFFRACplus Eva software verrsion 3.1. The thermal behaviour was examined using differential scanning calorimetry (DSC) Setaram LABSYS, (Caluire, France) with a constant heating rate of 10 K/min in an argon atmosphere. Magnetic measurements were carried out using a vibrating sample magnetometer (VSM) (Lake Shore VSM 7410, Westerville, OH, USA), with a maximum applied field of 20 kOe for M-H measurements at room temperature, and a constant field of 10 kOe for M-T measurements.

## 3. Results

Figure 1 displays the X-ray diffraction patterns of the as-spun $MM_{14}Fe_{80-x}Hf_xB_6$ (x = 0–3 at. %) ribbons, which were produced at wheel speeds of 35 m/s. The diffraction pattern corresponding to the sample without Hf addition shows some lines specific to the 2:14:1 crystalline phase, but more prominently, a broad bump around 43.5 degrees is observed. Such a bump is characteristic of amorphous structures, suggesting that the melt-spun ribbons contain a significant amount of amorphous phase. With the increase in Hf content, the bump widened and the diffraction lines faded, indicating that the volume fraction of the amorphous phase increases significantly; therefore, the addition of Hf can improve the glass-forming ability of the alloys.

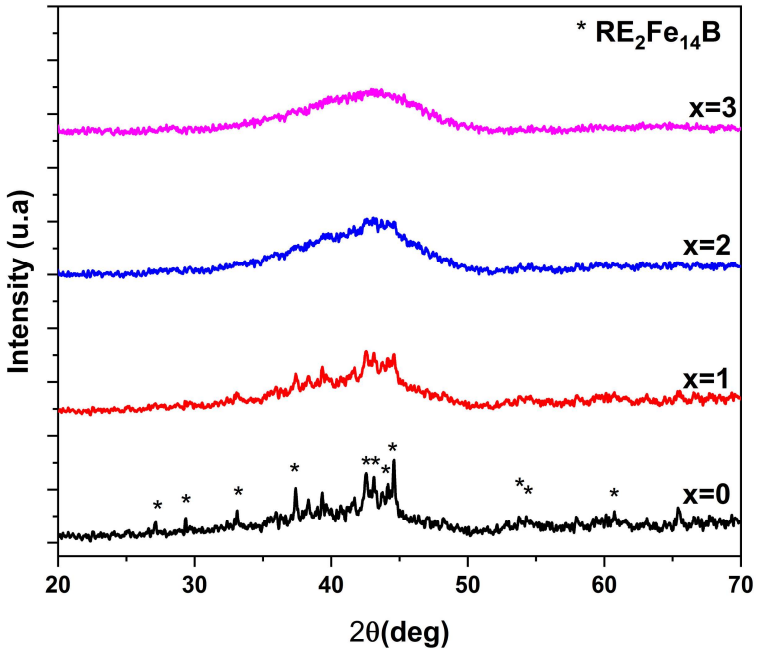


**Figure 1.** XRD patterns for as-spun $MM_{14}Fe_{80-x}Hf_xB_6$ (x = 0–3 at. %) ribbons.

Figure 2 below showcases the differential scanning calorimetry (DSC) graphs of the as-spun $MM_{14}Fe_{80-x}Hf_xB_6$ (x = 0–3 at. %) ribbons at a heating rate of 20 K/min.

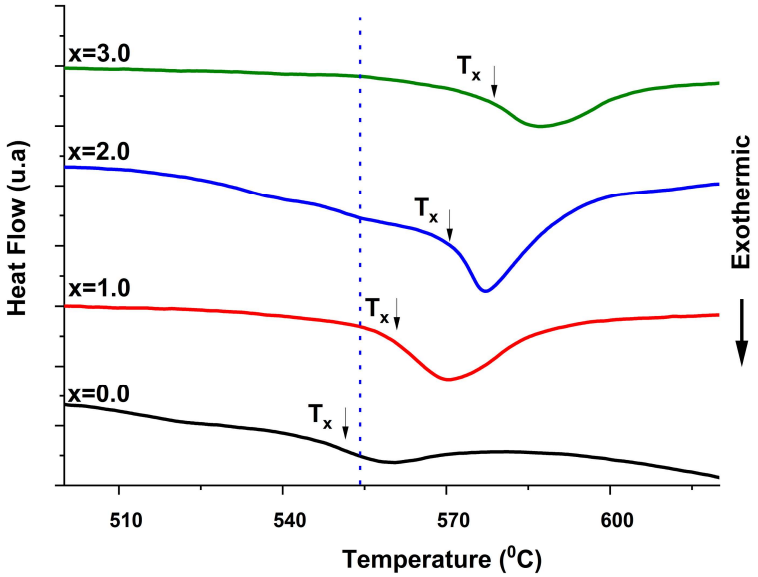


**Figure 2.** DSC curves for the as-spun $MM_{14}Fe_{80-x}Hf_xB_6$ (x = 0–3 at. %) ribbons (heated at 20 K/min).

DSC analysis of as-spun ribbons $MM_{14}Fe_{80-x}Hf_xB_6$ (x = 0–3 at. %) revealed an exothermic peak associated with the crystallization of the amorphous phase for all the studied bands. The presence of the amorphous phase is consistent with the XRD results presented in Figure 1. The temperatures ($T_x$) of the onset of the crystallization of the amorphous phase gradually increased from 557 °C to 583 °C, with the increase in the Hf content from 0 to 3 at. %, leading to the idea that the addition of Hf to $MM_{14}Fe_{80-x}Hf_xB_6$ has the effect of increasing the crystallization temperature of the bands. Such an effect of Hf was also reported in the case of addition to other materials such as $Fe_{57.2}Co_{30.8}Zr_{7-x}Hf_xB_4Cu_1$in [35]. It is well known that the magnetic characteristics of alloys from the RE-Fe-B system are closely related to their microstructure. Therefore, the implementation of an optimal isothermal treatment for amorphous as-cast ribbons, which would lead to an optimal microstructure (the formation and size of crystal grains) to counteract the negative impact of a possible uneven distribution of atomic elements and crystal nuclei, is imperatively necessary. Thus, after analyzing the crystallization temperatures of the amorphous phase from the DSC curves shown in Figure 2, a controlled thermal annealing process was applied to the amorphous bands in the temperature range of 550–690 °C. Here, the lower limit of 550 °C represents the temperature at which crystallization begins corresponding to ribbons with 0 at. % Hf, and the upper limit of 690 °C represents the end temperature of crystallization corresponding to the band with 3 at. % Hf. The annealing time was between 10 and 30 min for all ribbons. Depending on the Hf content of the ribbons, different optimal annealing conditions were found, namely 630 °C for 25 min for ribbons without Hf, 640 °C for 25 min for x = 1, 650 °C for 20 min for x = 2, and 660 °C for 15 min for x = 3.

Figure 3 shows the typical XRD patterns for the $MM_{14}Fe_{80-x}Hf_xB_6$ (x = 0–3 at. %) ribbons annealed under optimal annealing conditions. The analysis revealed the presence of both the 2:14:1 tetragonal phase (with space group P42/mnm) and the α-Fe phase (with space group Im3m), without other additional phases.

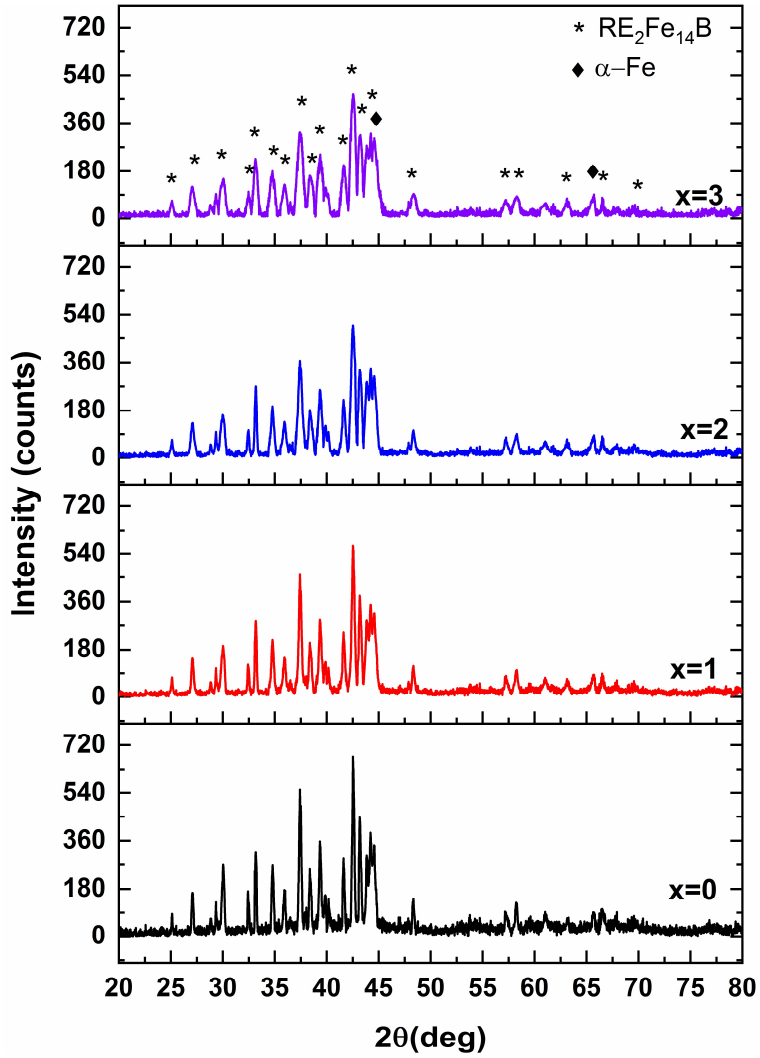


**Figure 3.** XRD patterns for optimal annealed $MM_{14}Fe_{80-x}Hf_xB_6$ (x = 0–3 at. %) ribbons.

With the increase in the Hf content, the intensity of the diffraction peaks decreases, becoming wider at the same time, indicating a decrease in the size of the crystalline grains. Indeed, according to the Debye–Scherrer equation, the crystalline grain size decreased from (68 ± 1.8) nm for the ribbons with x = 0 at. % Hf to (26 ± 1) nm for the ribbons with x = 3 at. % Hf. This suggests that the addition of Hf plays a crucial role in the refinement of hard magnetic grains. To investigate whether the addition of Hf atoms results in their inclusion in the 2:14:1 hard magnetic phase, the crystal lattice parameters were calculated using full spectrum fitting with Jade 6.0 software to the XRD patterns. The results are presented in Table 1.

**Table 1.** The lattice constants of the 2:14:1 $MM_{14}Fe_{80-x}Hf_xB_6$ (x = 0–3.0 at. %) ribbons.

| X (at. %) | a (Å) | b (Å) |
|---|---|---|
| 0 | 8.7636 ± 0.0002 | 12.1815 ± 0.0003 |
| 1.0 | 8.7636 ± 0.0003 | 12.1845 ± 0.0002 |
| 2.0 | 8.7690 ± 0.0002 | 12.1864 ± 0.0002 |
| 3.0 | 8.7614 ± 0.0001 | 12.1865 ± 0.0003 |

It can be seen that the lattice parameters remain largely unchanged with increasing Hf content from 0 to 3.0 at. %, which means that Hf cannot enter the 2:14:1 hard magnetic phase to substitute for Fe. If the Hf atoms were to occupy the Fe sites within the main

phase lattice, the lattice constants would increase and the diffraction peaks would migrate to smaller angles in accordance with the Bragg equation: $n\lambda = 2d\sin\theta$, with dHf = 2.16 Å and dFe = 1.72 Å. However, the lack of significant changes in the crystal lattice parameters further confirms that the Fe atoms in the main phase are not being replaced by Hf atoms. Despite this, no Hf-based phase was detected in the X-ray diffractions, most likely due to the small amount of Hf added. A similar behaviour was noticed by Rehman [36], who reported that Ta may not be detected directly unless it forms large inclusions in Nd-Fe-B-type alloys. To clarify the effect of the Hf element on the morphology of the MM-Fe-Hf-B ribbon samples, SEM images of the ribbons were obtained and are shown in Figure 4a–d. The average grain dimensions were determined using ImageJ software version 1.54.

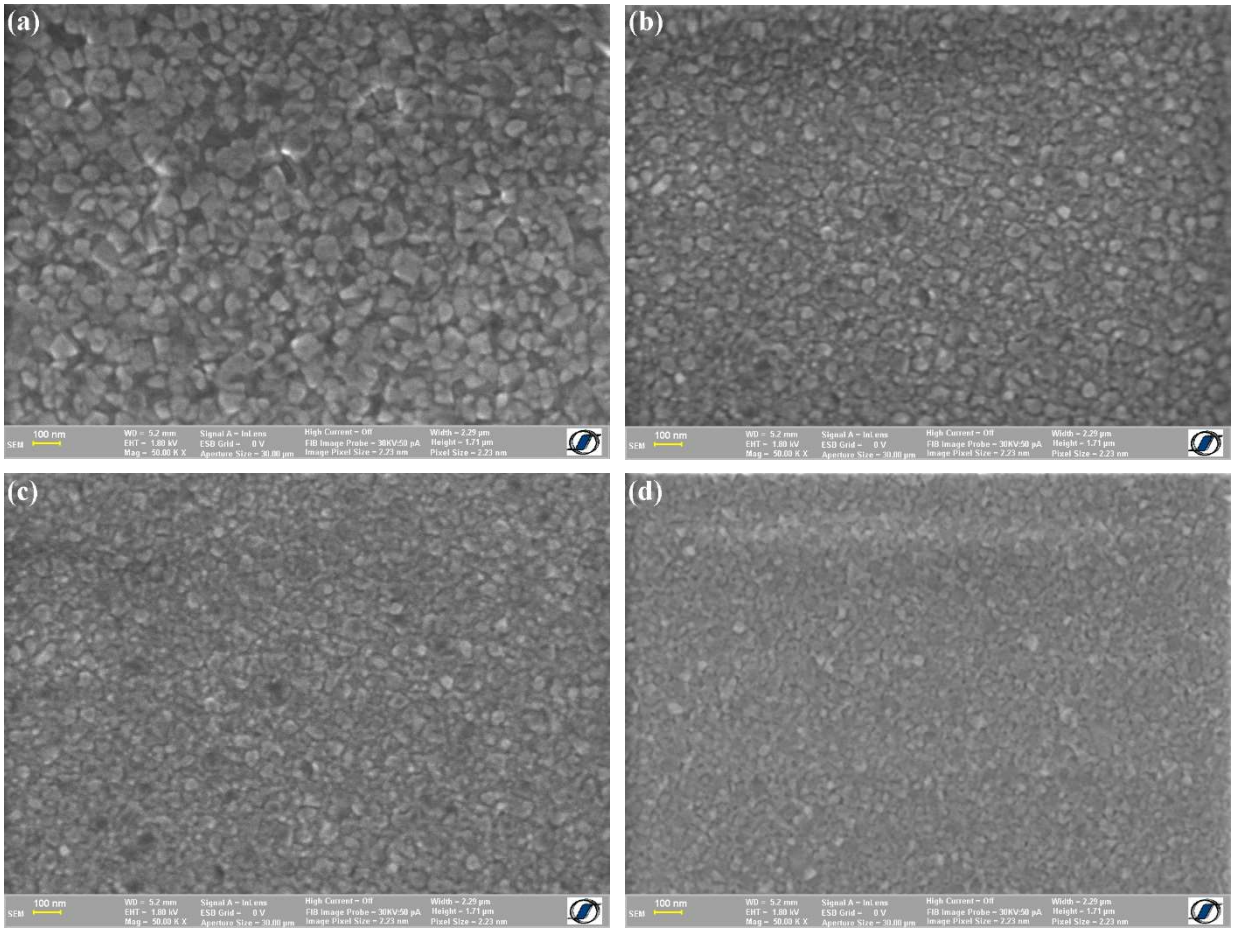


**Figure 4.** SEM images of the $MM_{14}Fe_{80-x}Hf_xB_6$ ribbons: (**a**) x = 0, (**b**) x = 1.0, (**c**) x = 2.0, and (**d**) x = 3.0 at. %.

The ribbons with Hf = 0 at. %, have an average grain size of (60 ± 2) nm, showing a non-uniform microstructure with grain sizes ranging from (20 ± 2) nm to (110 ± 2) nm. With the addition of Hf, both a reduction in the average grain size of the ribbon samples and a more uniform distribution of grain sizes are observed. Thus, for the sample with x= 3 at. % Hf, the average grain size decreased from (60 ± 2) nm to (20 ± 2) nm. The smallest grain size is (15 ± 2) nm and the largest grain size is (50 ± 2) nm. Therefore, the SEM results highlight the role of Hf in refining the grain structure of the ribbon samples, confirming the XRD-ray diffraction findings. It is important to point out that the grain-refining impact of Hf was more pronounced in the ribbon sample containing a higher concentration of Hf.

The evolution of the magnetic properties of the $MM_{14}Fe_{80-x}Hf_xB_6$ (x = 0–3 at. %) ribbons annealed at optimal conditions depending on the Hf content is illustrated in Figure 5.

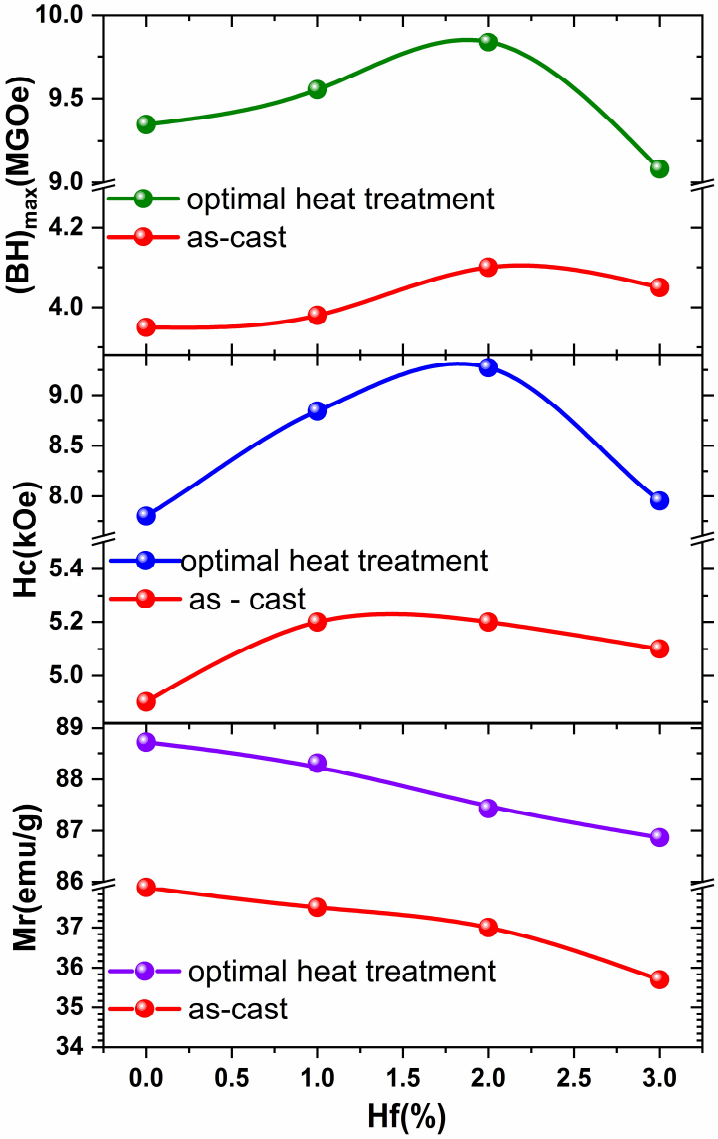


**Figure 5.** The evolution of the magnetic properties of the $MM_{14}Fe_{80-x}Hf_xB_6$ (x = 0–3 at. %) ribbons annealed at optimal conditions vs. the Hf content, and the red point represents the value corresponding to the as-cast ribbons with 2 at. % Hf.

The progressive inclusion of Hf in the material leads to a decrease in the remanent magnetization (Mr), as the saturation magnetization (Ms) decreases due to the presence of non-magnetic Hf. However, there is an enhancement in the coercive field (Hc) as the Hf content increases, which can be attributed to the reduction in the crystalline grain size. Additionally, the improvement in Hc may also result from a more uniform microstructure and homogeneous grain boundaries facilitated by the addition of Hf. The maximum energy product, $(BH)_{max}$, shows an initial increase with the increase in Hf content up to x = 2 at. %, after which it starts to decrease due to the trade-off between the reduction in Mr and the increase in Hc. The optimal magnetic properties, including Mr = 87 emu/g, Hc = 9.25 kOe, and $(BH)_{max}$ = 9.75 MGOe, were achieved for x = 2 at. %. Therefore, we can conclude that it is crucial to carefully control the amount of Hf added to achieve the desired magnetic properties. To evaluate the impact of Hf addition on the Curie temperature (Tc) on the ribbons, thermomagnetic measurements were employed in the temperature range of 50–400 °C under a magnetic field of 10 kG, with a heating rate of 2 °C/min. Figure 6a shows the M vs. T curves; in the inset, the corresponding $\delta M/\delta T$ curves are shown. The Curie temperature is determined from the minima of the $\delta M/\delta T$ curves, and its evolution

against the Hf content is illustrated in Figure 6b. The results of these investigations show that Tc remains almost unchanged with increasing Hf content. This behaviour confirms that Hf does not enter the 2:14:1 main phase. Otherwise, due to the difference between the atomic radius of the Hf and Fe, the interatomic distance between the Fe atoms in the crystalline cell would change, leading to changes in interactions between them and implicitly to the variations in Tc.

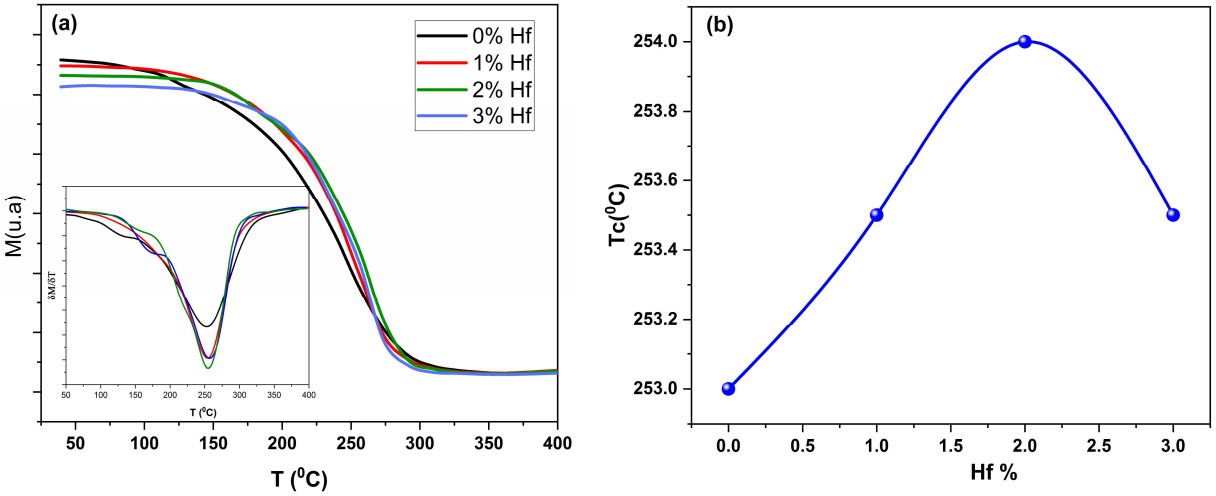


**Figure 6.** The thermomagnetic curves with their derivative of $MM_{14}Fe_{80-x}Hf_xB_6$ (x = 0–3.0) ribbons (**a**) and Tc variation vs. Hf content (**b**).

The thermal stability of the studied samples was investigated by means of the temperature coefficients (α) of the remanence and (β) of the coercivity, the coefficients, which represent the rate of variation in the remanence, Mr, respectively of the coercivity, Hc, in a temperature range specified. These coefficients α and β are defined by the following relations:

$$\alpha = \frac{M_r(T_2) - M_r(T_1)}{[M_r(T_1)(T_2 - T_1)]} \times 100\% \quad \beta = \frac{H_c(T_2) - H_c(T_1)}{[H_c(T_1)(T_2 - T_1)]} \times 100\%$$

where $M_r(T_2)$, $M_r(T_1)$ and $H_c(T_2)$, $H_c(T_1)$ are remanence, respectively coercivity at the final temperature, $T_2$, respectively at the initial temperature $T_1$.

Figure 7 shows the evolution of α and β temperature coefficients of the $MM_{14}Fe_{80-x}Hf_xB_6$ ribbons (x = 0–3.0 at. %) with the Hf content in the temperature range of 25–150 °C.

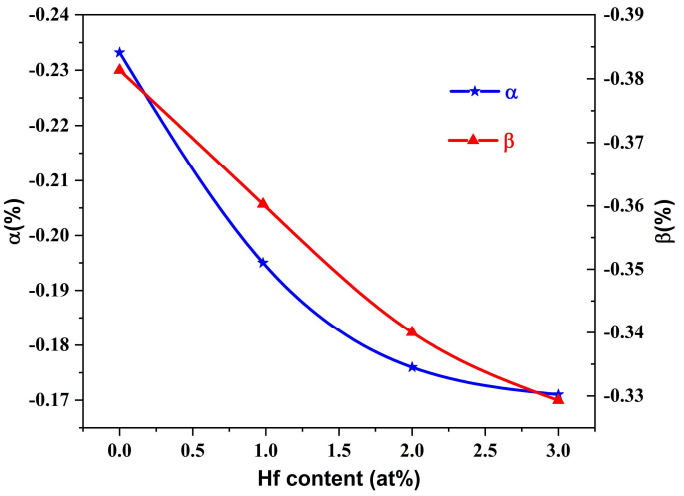


**Figure 7.** Evolution of remanence temperature coefficient α and coercivity temperature coefficient β of the $MM_{14}Fe_{80-x}Hf_xB_6$ ribbons (x = 0–3.0 at. %) with the Hf content in the range 25–150 °C.

Increasing the Hf content from 0 to 3 at. % in the $MM_{14}Fe_{80-x}Hf_xB_6$ ribbons leads to a decrease in coefficient values from $(-0.233 \pm 0.004)\%/^{\circ}C$ to $(-0.171 \pm 0.002)\%/^{\circ}C$ for $\alpha$, while $\beta$ decreases from $(-0.381 \pm 0.004)\%/^{\circ}C$ to $(-0.329 \pm 0.003)\%/^{\circ}C$. This behaviour of $\alpha$ and $\beta$ coefficients indicates that both the thermal stability of the remanence and of the coercivity are sensitive to the addition of Hf, more precisely, the thermal stability can be improved by controlling the Hf content.

## 4. Conclusions

The present research demonstrates that the addition of a very small amount of Hf in the $MM_{14}Fe_{80-x}Hf_xB_6$ ribbons has significant beneficial effects on their magnetic properties. The merits of Hf are related to the improvement of the coercivity, energy product, and thermal stability, due to efficient microstructure modification. In fact, the addition of non-magnetic Hf leads to a refinement of the size of the crystalline grains of the main phase $RE_2Fe_{14}B$ and also to a uniformity of the size of these crystalline grains. As a result, the coercivity and energy product increase with increasing Hf content up to 2 at. %, while the remanence decreases continuously due to dilution with non-magnetic elements. The thermal stability is improved by an enhancement of the remanence temperature coefficient, $\alpha$, from $(-0.233 \pm 0.004)\%/^{\circ}C$ to $(-0.171 \pm 0.002)\%/^{\circ}C$, and of coercivity temperature coefficient, $\beta$, from $(-0.381 \pm 0.004)\%/^{\circ}C$ to $(-0.329 \pm 0.003)\%/^{\circ}C$, when the Hf content increases from 0 to 3 at. %. The best combination of magnetic properties such as coercivity, Hc = 9.25 kOe, Mr = 87 emu/g, and $(BH)_{max}$ = 9.45 MGOe was obtained for Hf content x = 2 at. %. The XRD investigations showed that Hf does not enter the crystalline network of the main phase and therefore has no influence on the Curie temperature. Thus, through the prism of the obtained results, we can state that the future use of $MM_{14}Fe_{78}Hf_2B_6$ ribbons as precursors for the preparation of permanent magnets represents a viable alternative to permanent magnets with high magnetic performance and low costs.

**Author Contributions:** M.L.: Conceptualization, Sample preparation, Writing—original draft, Experiments, Investigation, Methodology, and Resources. M.G.: Supervision, Funding acquisition, Writing—review and editing. G.B.: Sample preparation and Investigation, G.A.: Investigation and Methodology. G.S.: Validation, Formal analysis. Investigation, and Methodology. L.C.B.: Experiments and Methodology. T.R.: XRD analysis, Phase identification. N.L.: Supervision, Funding acquisition, Writing—review and editing. All authors have read and agreed to the published version of the manuscript.

**Funding:** This research was financially supported by a grant of the Ministry of Research, Innovation and Digitization, CNCS–UEFISCDI, project number PN-III-P1-1.1-TE-2021-0976, within PNCDI III.

**Data Availability Statement:** The raw data supporting the conclusions of this article will be made available by the authors on request.

**Conflicts of Interest:** The authors declare no conflicts of interest.

## References

1. Gutfleisch, O.; Willard, M.A.; Brück, E.; Chen, C.H.; Sankar, S.; Liu, J.P. Magnetic Materials and Devices for the 21st Century: Stronger, Lighter, and More Energy Efficient. *Adv. Mater.* **2011**, *23*, 821–842. [CrossRef] [PubMed]
2. Pathak, A.K.; Khan, M.; Gschneidner, K.A., Jr.; McCallum, R.W.; Zhou, L.; Sun, K.; Dennis, K.W.; Zhou, C.; Pinkerton, F.E.; Kramer, M.J. Cerium: An Unlikely Replacement of Dysprosium in High Performance Nd–Fe–B Permanent Magnets. *Adv. Mater.* **2015**, *27*, 2663–2667. [CrossRef] [PubMed]
3. Skokov, K.P.; Gutfleisch, O. Heavy rare earth free, free rare earth and rare earth free magnets-Vision and reality. *Scr. Mater.* **2018**, *154*, 289–294. [CrossRef]
4. Sugimoto, S. Current status and recent topics of rare-earth permanent magnets. *J. Phys. D Appl. Phys.* **2011**, *44*, 064001. [CrossRef]
5. Pavel, C.C.; Tzimas, E. *Raw Materials in the European Defence Industry*; Publications Office of the European Union: Luxembourg, 2016; Available online: https://publications.jrc.ec.europa.eu/repository/handle/JRC98333 (accessed on 11 November 2016).
6. Gimaev, R.R.; Komlev, A.S.; Davydov, A.S.; Kovalev, B.B.; Zverev, V.I. Magnetic and Electronic Properties of Heavy Lanthanides (Gd, Tb, Dy, Er, Ho, Tm). *Crystals* **2021**, *11*, 82. [CrossRef]
7. Binnemans, K.; Jones, P.T.; Müller, T.; Yurramendi, L. Rare Earths and the Balance Problem: How to Deal with Changing Markets? *J. Sustain. Metall.* **2018**, *4*, 126–146. [CrossRef]

8. Goodenough, K.M.; Wall, F.; Merriman, D. The Rare Earth Elements: Demand, Global Resources, and Challenges for Resourcing Future Generations. *Nat. Resour. Res.* **2017**, *27*, 201–216. [CrossRef]
9. Li, Z.B.; Shen, B.G.; Zhang, M.; Hu, F.X.; Sun, J.R. Substitution of Ce for Nd in preparing $R_2Fe_{14}B$ nanocrystalline magnets. *J. Alloys Compd.* **2015**, *628*, 325–328. [CrossRef]
10. Liu, W.; Zhang, Z.; Yue, M.; Li, Z.; Wu, D.; Zhou, Z.; Chen, H.; Li, Y.; Pang, Z.; Yu, X. MM-Fe-B based gap magnet with excellent energy density. *Intermetallics* **2019**, *115*, 106626. [CrossRef]
11. Gabay, A.M.; Hadjipanayis, G.C. Recent developments in $RFe_{12}$-type compounds for permanent magnets. *Scr. Mater.* **2018**, *154*, 284–288. [CrossRef]
12. Ahmad, Z.; Waqas, M.; Ali, Z.A. Fabrication and analysis of mischmetal MM-Fe-B magnetic alloy. *J. Magn. Magn. Mater.* **2022**, *553*, 169257. [CrossRef]
13. Jin, J.; Ma, T.; Zhang, Y.; Bai, G.; Yan, M. Chemically Inhomogeneous RE-Fe-B Permanent Magnets with High Figure of Merit: Solution to Global Rare Earth Criticality. *Sci. Rep.* **2016**, *6*, 32200. [CrossRef] [PubMed]
14. Chang, H.W.; Chen, C.H.; Chang, C.W.; Hsieh, C.C.; Guo, Z.H.; Chang, W.C. High magnetic properties of nanocomposite ribbons made with Mischmetals–Fe–Co–Ti–B alloys. *J. Appl. Phys.* **2009**, *105*, 07A704. [CrossRef]
15. Zhang, M.; Liu, Y.; Li, Z.B.; Peng, L.C.; Shen, B.G.; Hu, F.X.; Sun, J.R. Magnetization process of nanocrystalline mischmetal-Fe-B ribbons. *J. Alloys Compd.* **2016**, *688*, 1053–1057. [CrossRef]
16. Quan, N.T.; Luo, Y.; Yan, W.L.; Yuan, C.; Yu, D.B.; Sun, L.; Lu, S.; Li, H.W.; Zhang, H.B. Hard magnetic properties and coercivity mechanism of melt-spun Misch Metal-Fe-B alloy. *J. Magn. Magn. Mater.* **2017**, *437*, 12–16. [CrossRef]
17. Li, Z.B.; Wang, L.C.; Geng, X.P. Variation of magnetic properties with mischmetal content in the resource saving magnets of MM-Fe-B ribbons. *J. Magn. Magn. Mater.* **2017**, *426*, 70–73. [CrossRef]
18. Chang, H.W.; Chen, C.H.; Hsieh, C.C.; Chang, W.C. Magnetic Properties of Melt Spun Mischmetals-Fe-Ti-B Nanocomposite Ribbons. *J. Nanosci. Nanotechnol.* **2011**, *11*, 2756. [CrossRef] [PubMed]
19. Li, Z.B.; Li, Y.; Liu, Z.X.; Li, Y.F.; Zhang, X.F. Improving magnetic properties in mischmetal-based sintered composite magnets by regulating element distribution. *AIP Adv.* **2019**, *9*, 075109. [CrossRef]
20. Zhang, Z.; Sharma, P.; Yubuta, K. Synthesis, microstructure and magnetic properties of low Nd content $Fe_{90}Nd_5B_{3.5}M_{1.5}$ (M = Hf, Ti and Ta) alloys. *J. Appl. Phys.* **2012**, *111*, 07B501. [CrossRef]
21. Zhong, M.; Tao, L.; Wu, T.; Zhang, Q.; Liu, R.; Zhong, Z.; Rehman, S.U. Tailoring the magnetic properties and microstructure of NdFeB ribbon alloys by Hf addition. *J. Alloys Compd.* **2021**, *876*, 160197. [CrossRef]
22. Zhang, L.; Jiang, Q.; Quan, L.W.; Rehman, S.U.; Lei, W.; He, L.; Zeng, Q.; Hu, X.; Liu, R.; Zhong, Z. Effects of Hf addition on the microstructure, magnetic properties and coercivity mechanism of Nd-Ce-Fe-B ribbons fabricated by melt-spinning technique. *J. Magn. Magn. Mater.* **2019**, *474*, 305–310. [CrossRef]
23. Chang, H.W.; Huang, S.T.; Chang, C.W.; Chiu, C.H.; Chen, I.W.; Chang, W.C.; Sun, A.C.; Yao, Y.D. Effect of additives on the magnetic properties and microstructure of melt spun $SmCo_{6.9}Hf_{0.1}M_{0.1}$ (M = B, C, Nb, Si, Ti) ribbons. *J. Alloys Compd.* **2008**, *455*, 506–509. [CrossRef]
24. Zhang, Z.; Jin, J.; Liang, L. High-performance Nd-Fe-B sintered magnets via co-doping high-melting-point Zr and low-melting-point $Dy_{71.5}Fe_{28.5}$. *J. Magn. Magn. Mater.* **2019**, *487*, 165356. [CrossRef]
25. Rieger, G.; Seeger, M.; Sun, L.; Kronmuller, H. Micromagnetic analysis applied to melt-spun NdFeB magnets with small additions of Ga and Mo. *J. Magn. Magn. Mater.* **1995**, *151*, 193–201. [CrossRef]
26. Derewnicka-Krawczynska, D.; Ferrari, S.; Bilovol, V. Influence of Nb, Mo, and Ti as doping metals on structure and magnetic response in NdFeB based melt spun ribbons. *J. Magn. Magn. Mater.* **2018**, *462*, 83–95. [CrossRef]
27. Zhang, L.L.; Song, J.; Rehman, S.U. Uneven Evolution of Microstructure, Magnetic Properties and Coercivity Mechanism of Mo-Substituted Nd–Ce–Fe–B Alloys. *Acta Metall. Sin.* **2021**, *34*, 590–596. [CrossRef]
28. Raja, A.; Adhikary, T.; Al-Omari, I.A.; Das, G.P.; Ghosh, S.; Satapathy, D.K.; Oraon, A.; Shield, J.E.; Aich, S. Rapidly solidified Sm-Co-Hf-B magnetic Nano-composites: Experimental and DFT studies. *J. Magn. Magn. Mater.* **2020**, *504*, 166645. [CrossRef]
29. Zhong, M.; Xie, W.; Rehman, S.U. Magnetic Properties and Microstructural Modifications of Sm-Co-Hf Alloy Ribbons by B Addition. *J. Supercond. Nov. Magn.* **2022**, *35*, 1329–1335. [CrossRef]
30. Torres, C.E.R.; Saccone, F.D.; Sanchez, F.H. Magnetic anisotropy induced in $Nd_{16}Fe_{76}B_8$ by Hf additions. *Phys. B Condens. Matter* **2002**, *320*, 308–311. [CrossRef]
31. Chang, H.W.; Huang, S.T.; Chang, C.W.; Chiu, C.H.; Chen, I.W.; Chang, W.C.; Sun, A.C.; Yao, Y.D. Comparison on the magnetic properties and phase evolution of melt-spun $SmCo_7$ ribbons with Zr and Hf substitution. *Scr. Mater.* **2007**, *56*, 1099–1102. [CrossRef]
32. Zheng, Q.; Jiang, M.L.; Quan, Q.C.; Zhang, J.S.; Zhang, Z.C. Striking effect of Hf addition on magnetic properties and thermal stability of $Nd_{13}Fe_{81-x}B_6Hf_x$ (x = 0–1.0) alloys. *J. Alloys Compd.* **2016**, *688*, 363–367. [CrossRef]
33. Grigoras, M.; Lostun, M.; Stoian, G.; Herea, D.D.; Chiriac, H.; Lupu, N. Microstructure and magnetic properties of Ce10+xFe84−xB6 nanocrystalline ribbons versus preparation conditions. *J. Magn. Magn. Mater.* **2017**, *432*, 119–123. [CrossRef]
34. Grigoras, M.; Lostun, M.; Borza, F.; Porcescu, M.; Lupu, N. The effect of the Mo addition on the magnetic properties and phase constituents of the Ce-(FeCo)–B ribbons. *Intermetallics* **2022**, *141*, 107425. [CrossRef]

35. Srivastava, A.P.; Babu, D.A.; Verma, A.; Deshmukh, A.A.; Kaushal, A.; Palikundwar, U.A. Understanding the effect of Hf on thermal stability and glass forming ability of $Fe_{57.2}Co_{30.8}Zr_{7-x}Hf_xB_4Cu_1$ (x = 3, 5, and 7) metallic glasses. *J. Non-Cryst. Solids* **2019**, *503–504*, 7–12. [CrossRef]
36. Rehman, S.U.; Jiang, Q.; Lei, W.; Zeng, L.; Tan, Q.; Ghazanfar, M.; Awan, S.U.; Ahmad, T.; Zhong, M.; Zhong, Z. Microstructure, magnetic properties, thermal stabilities and coercivity mechanisms of Ta doped Nd-Fe-B ribbons. *J. Phys. Chem. Solids* **2019**, *124*, 261–265. [CrossRef]

**Disclaimer/Publisher's Note:** The statements, opinions and data contained in all publications are solely those of the individual author(s) and contributor(s) and not of MDPI and/or the editor(s). MDPI and/or the editor(s) disclaim responsibility for any injury to people or property resulting from any ideas, methods, instructions or products referred to in the content.